Experimental evaluation of terrestrial LiDAR-based surface roughness estimates

Ryan M. Pollyea and Jerry P. Fairley
Department of Geological Sciences, University of Idaho, Moscow, Idaho 83844-3022, USA

ABSTRACT

The rapid proliferation of portable, ground-based light detection and ranging (LiDAR) instruments suggests the need for additional quantitative tools complementary to the commonly invoked digital terrain model (DTM). One such metric is surface roughness, which is a measure of local-scale topographic variability and has been shown to be effective for mapping discrete morphometric features, i.e., fractures in outcrop, landslide scarps, and alluvial fan deposits, to name a few. Several surface roughness models have been proposed, the most common of which is based on the standard deviation of point distances from a reference datum, e.g., DTM panels or best-fit planes. In the present work, we evaluate the accuracy of these types of surface roughness models experimentally by constructing a surface of known roughness, acquiring terrestrial LiDAR scans of the surface at 25 dual-axis rotations, and comparing surface roughness estimates for each rotation calculated by three surface roughness models. Results indicate that a recently proposed surface roughness model based on orthogonal distance regression (ODR) planes and orthogonal point-to-plane distance measurements is generally preferred on the basis of minimum error surface roughness estimates. In addition, the effects of terrestrial LiDAR sampling errors are discussed with respect to this ODR-based surface roughness model, and several practical suggestions are made for minimizing these effects. These include (1) positioning the laser scanner at the largest reasonable distance from the scanned surface, (2) maintaining half-angles for individual scans at less than 22.5°, and (3) minimizing occlusion (shadowing) errors by using multiple, merged scans with the least possible overlap.

INTRODUCTION

Light detection and ranging (LiDAR) or laser swath mapping has become an invaluable tool for researchers investigating earth surface processes. Originally implemented for mapping Earth's surface from an aerial platform, LiDAR has dramatically reshaped morphometric investigations in fields such as coastal erosion, forest management, hazard assessment, and glacier monitoring, to name a few (Wehr and Lohr, 1999). More recently, portable, ground-based LiDAR systems (also known as terrestrial laser scanners) have become accessible to the research community and are being lauded for their ability to render fine-scale detail with respect to outcrop mapping (Bellian et al., 2005; Buckley et al., 2008) and river channel deposits (Aberle and Nikora, 2006; Heritage and Milan, 2009). The primary tool used for analyzing high-resolution LiDAR-derived point data is the digital terrain model (DTM), which, in various forms, is a signal processing filter used to define a continuous surface that is representative of the mapped ground surface (Liu, 2004). Although the DTM is a powerful tool for morphometric analysis, some information is lost in the filtering process; therefore, a natural extension for the maturation of LiDAR data analysis is the development of complementary tools suitable for extracting higher-order information from the point-cloud data. One such metric is surface roughness.

As the name suggests, surface roughness is a measure of local topographic variability and has been used broadly in the geosciences for mapping discrete features that can be smoothed over by DTM analysis. For example, surface roughness has been shown to be an effective tool for mapping landslide scarps (McKean and Roering, 2004), channel bed morphology (Cavalli et al., 2008), alluvial fan units (Frankel and Dolan, 2007), fault surface features (Sagy et al., 2007), and fractures in exposed outcrops (Pollyea and Fairley, 2011). In terms of LiDAR analysis, surface roughness models have seen a number of variants, but they are commonly invoked as a digital signal filter for mapping morphometric features that are lost with DTM smoothing functions. For example, McKean and Roering (2004) defined surface roughness as the degree of normal vector clustering over gridded DTM panels; however, the authors acknowledged that this method suffered from scale-dependent errors for smooth surfaces. Similarly, Frankel and Dolan (2007) defined surface roughness as the standard deviation of slope over a moving window. More commonly, surface roughness has been defined, for a gridded data set, as the standard deviation of point elevations above a reference datum, such as a DTM (Glenn et al., 2006; Cavalli et al., 2008; Sankey et al., 2010) or best-fit plane (Fardin et al., 2004; Aberle and Nikora, 2006; Sagy et al., 2007). Although each of these latter surface roughness models uses different DTM methods, the shared feature is that surface roughness is modeled as a variation of elevation from a reference datum. The suitability of surface roughness models developed as a function of point-to-datum distances with respect to one coordinate direction (i.e., elevation) was discussed in Pollyea and Fairley (2011), where we demonstrate that surface roughness models of this type may be prone to error resulting from contamination due to residual topography. In response, we proposed a surface roughness model, for a gridded point-cloud data set, that uses orthogonal distance regression (ODR) to construct local (grid cell) reference datum and models the surface roughness of each grid cell as the standard deviation of orthogonal point-to-plane distances.

In Pollyea and Fairley (2011), the surface roughness errors were defined as the absolute difference between the ODR-based roughness estimates and a similar surface roughness model that fits grid-cell reference planes by ordinary least-squares (OLS) regression and models surface roughness as the standard deviation of point-to-plane distances measured with respect to the dependent coordinate axis. Although this method for error quantification is reasonable on a mathematical basis, the inherent assumption is that the ODR-based surface roughness estimates contain negligible errors. In the present work, we discard this assumption and evaluate the ODR-based roughness model for accuracy with respect to an experimental surface of known surface roughness. Individual LiDAR scans are obtained

Geosphere; February 2012; v. 8; no. 1; p. 222–228; doi:10.1130/GES00733.1; 7 figures; 1 table.

for the experimental surface at 25 combinations of dual-axis rotations between 0 and 45 degrees from the scanner-normal vertical plane. Two additional surface roughness models are included in this analysis: (1) the aforementioned OLS-based surface roughness model and (2) a "hybrid" surface roughness model that uses ODR reference datum and models surface roughness as the standard deviation of point-to-plane distances measured with respect to the dependent coordinate axis. The inclusion of these two models permits discussion of surface roughness errors as a function of reference datum and the orientation of point-to-plane distance measurements (orthogonal or axis-dependent).

METHODS

The methods used in this experiment are: (1) constructing an experimental surface, (2) calculating the theoretical roughness of the experimental surface, and (3) obtaining ground-based LiDAR scans of the experimental surface for combinations of dual-axis rotations between 0 and 45 degrees from a baseline reference orientation defined below.

Experimental Surface

An experimental surface was constructed using a 1 m by 1 m section of 0.019 m (3/4 in) thick plywood. Imperfections in the surface were filled with sandable wood putty and smoothed with a power sanding tool. The board was stored indoors under heavy weight to remove curvature. The prepared surface was overlaid with a 0.050 m regular grid and spherical roughness elements (table tennis balls) with 0.038 m diameter were placed at 132 randomly selected grid nodes. The table tennis balls were set in the board with adhesive caulk allowing a hemispherical protrusion above the board surface (Fig. 1A). Grid nodes receiving roughness elements were selected using a 0–1 random number generator (Press et al., 1992, ran0, p. 270–271); random (x,y) coordinates pairs were generated and shifted down to the nearest grid node, e.g., $x_{node} = x - x \bmod 0.050$. Upon completion, the experimental surface was painted with a flat white indoor/outdoor acrylic paint to achieve, as near as possible, equal specular reflection across the surface. The experimental surface was then mounted on a 0.038 m (1.5 in) steel pipe centered horizontally across the board to allow rotation about the surface-parallel horizontal axis. The experimental surface was mounted to a timber frame such that the finished experimental surface was forward facing with no surface occlusion upon dual-axis rotation (Fig. 1B).

Theoretical Surface Roughness

With complete knowledge of the experimental surface dimensions and the geometry and spatial distribution of the roughness elements, the theoretical surface roughness can be evaluated numerically. A randomized synthetic point cloud, representing an error-free LiDAR scan of the experimental surface, was generated and the solution for surface roughness was found by Monte Carlo simulation for increasing numbers of (x,y,z) coordinate triples. The synthetic point cloud is based on the geometric relationship between randomly generated (x,y) coordinate pairs and the fully dependent out-of-plane z-coordinate:

$$z = \begin{cases} \sqrt{r^2 - (x - x_{node})^2 - (y - y_{node})^2}, & (x,y) < |r| \text{ from node} \\ 0, & \text{otherwise} \end{cases}. \quad (1)$$

In Equation (1), x_{node} and y_{node} represent a nodal center for each of the 132 roughness elements on the experimental surface, and r is the roughness element radius, in this case 0.019 m. In other words, each randomly generated (x,y) pair is tested for proximity to a node center; if the point is within one ball radius of a node, then z is determined using the quadratic equation for a spherical surface; otherwise z is zero (Fig. 2A). This process was encoded in a FORTRAN 2003 program, and the surface roughness was calculated cumulatively (every 500,000 points) as the standard deviation of point distances from the mean z-plane. For each iteration, the new surface roughness was compared to the value from the previous iteration, and the solution was accepted for a convergence threshold of 1.0E-09 m. Convergence was obtained after generating 355,000,000 (x,y,z) coordinate triples, and the calculated theoretical roughness (σ_{thr}) of the experimental surface was estimated to be 3.60756E-03 m (Fig. 2B). For subsequent analysis, σ_{thr} represents an error-free statement (to the decimal precision of the Monte Carlo simulation) of the experimental surface roughness and will be used as the standard against which each surface roughness model is measured, i.e., σ_{thr} is free of angular scanning error, occlusion error, instrument precision error, analytical method error, and experimental error.

Data Acquisition

Laser scanning was performed in the Computational Hydrology Laboratory at the University of Idaho on April 2, 2011, using a Leica ScanStation2 terrestrial LiDAR scanner. The LeicaScanstation2 is a portable

Figure 1. The experimental surface used for this research. (A) Digital image of author fixing roughness elements to the surface using adhesive caulk. (B) Digital image of the completed surface and timber frame.

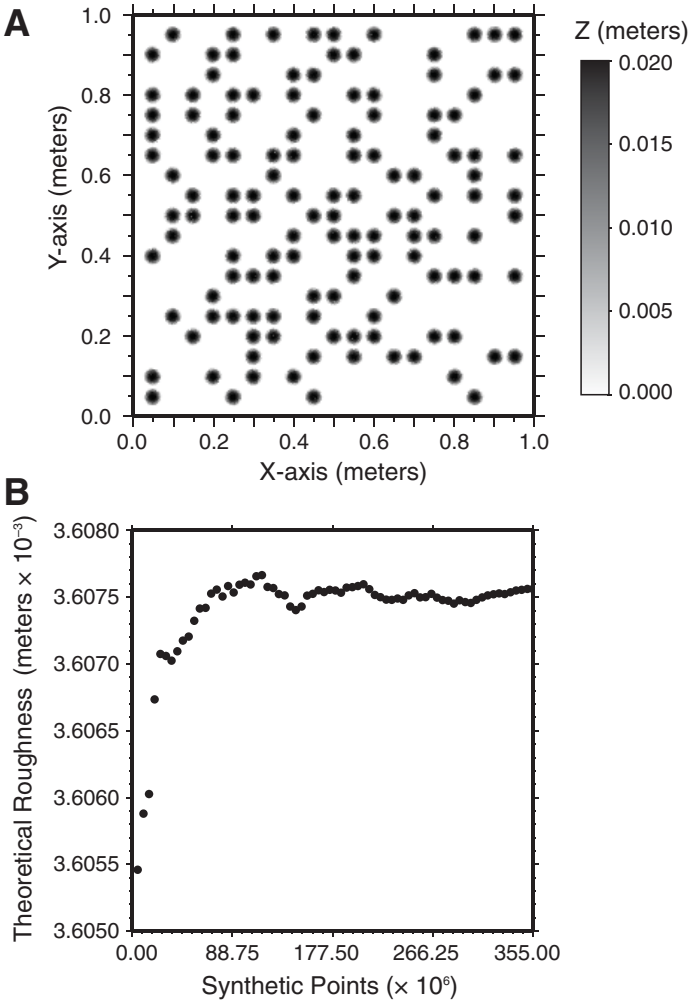

Figure 2. (A) Plot of the synthetic point cloud used for evaluating the theoretical roughness of the experimental surface. Note that (*x*,*y*) are plotted explicitly and *z* is shown in grayscale by orthogonal distance from the *xy*-plane. (B) Theoretical surface roughness showing convergence of the Monte Carlo solution.

terrestrial laser scanner operating with an acquisition rate of 50,000 points per second, maximum scan density of 1 mm at 1 m–50 m distance, and single datum position and distance accuracy of 6 mm and 4 mm, respectively. The experiment was arranged with the laser scanner 4.5 m from the experimental surface (Fig. 3A). In order to achieve the minimum scan-line distance across the entire experimental surface, and hence minimize angular sampling error, the scanner mirror and the center of the experimental surface were placed at equal elevations of 1.75 m from ground surface (Fig. 3B). The point acquisition spacing was set to 0.002 m horizontally and vertically at a range of 4.5 m (250,000 points per square meter).

Individual scans of the experimental surface were acquired for 25 dual-axis rotations. The dual-axis surface rotations are referenced by angles θ and ϕ, which correspond to angular rotation about the vertical and surface-parallel horizontal axes, respectively. Similarly, the notation σ(θ,ϕ) refers to the surface roughness estimate for the given dual-axis rotation. In order to fully define this reference system, the baseline orientation (θ = ϕ = 0°) must also be defined with respect to the scanner and experimental surface. Here we define the baseline surface orientation as the hypothetical vertical plane, the normal of which is parallel to the baseline reference scan line (Fig. 3). It follows that σ(0°,0°) refers to a surface roughness estimate corresponding to the experimental surface at the baseline orientation.

LiDAR scans of the experimental surface were acquired at 11.25° rotational intervals for each (θ,ϕ) combination between 0° and 45° (Figs. 3A and 3B). Following data acquisition, each data set was processed using Leica Cyclone v. 7 software to remove stray points. This was done by manually trimming points landing on surfaces beyond the extent of the experimental surface. Points in close proximity to the experimental surface, e.g., the plywood edge and adjacent timber frame, were filtered by specular intensity because the unpainted wood returned intensity values significantly below returns from the painted surface. The data set from each (θ,ϕ) LiDAR scan was exported as a raw point cloud in (*x*,*y*,*z*) format.

DATA ANALYSIS

The experimental surface roughness for each (θ,ϕ) rotation is evaluated using three models for surface roughness. Each surface roughness model is based on the common definition of surface roughness (σ) as the standard deviation of point distances (D) from a reference datum:

$$\sigma = \sqrt{\frac{1}{N}\sum_{i=1}^{N}\left(D_i - \bar{D}\right)^2}, \qquad (2)$$

where the overbar indicates the expected value (the mean). The features of the models evaluated here are the choice of reference datum and the orientation in which distances are measured from the datum. The reference planes used for this analysis are fit to the data by either ordinary least-squares regression (OLS) or orthogonal distance regression (ODR), the latter of which is also known as total least squares and errors-in-variables. Regression by OLS produces a best-fit plane by minimizing the sum of square point-to-plane distances with respect to the dependent principal axis, which, for this analysis, is the coordinate axis orthogonal to the baseline reference plane at θ = ϕ = 0°. In contrast, ODR produces a best-fit plane by minimizing the sum of square orthogonal point-to-plane distances. For point-to-plane distance measurements, two choices are considered: (1) orthogonal distance to the plane and (2) distance to the plane in the direction of the dependent coordinate axis (Fig. 4).

The three surface roughness models evaluated here are: (1) the ODR-based model (σ_{odr}) proposed by Pollyea and Fairley (2011), (2) an OLS-based model (σ_{ols}), and (3) a hybrid model (σ_{hyb}) with shared properties of σ_{odr} and σ_{ols}. The σ_{odr} model fits the reference datum by ODR and evaluates surface roughness as a function of orthogonal point-to-plane distances, whereas the σ_{ols} model fits reference datum by OLS regression and evaluates point-to-plane distance in the direction of the dependent axis. The σ_{hyb} model fits the reference datum by ODR, but evaluates point-to-plane distances in the same manner as the σ_{ols} model. The σ_{ols} and σ_{hyb} model are conceptually similar to those models that fit a DTM to the data and evaluate surface roughness as a function of elevation above the DTM. The σ_{hyb} model is included in the analysis to investigate the sensitivity of elevation-based surface roughness models to the choice of reference datum fitting procedure.

The surface roughness estimates of the experimental surface for each model and (θ,ϕ) rotation were computed using programs written in FORTRAN 2003. Although these surface roughness models are intended for use over a gridded data set, here the σ(θ,ϕ) for each model is analyzed without segmentation, i.e., the point cloud from each scan is analyzed as a single grid cell. Our analysis indicates the σ_{odr} roughness model returns consistent roughness values for all (θ,ϕ) rotations, with modestly decreasing roughness values at large deviation from the baseline orientation. In

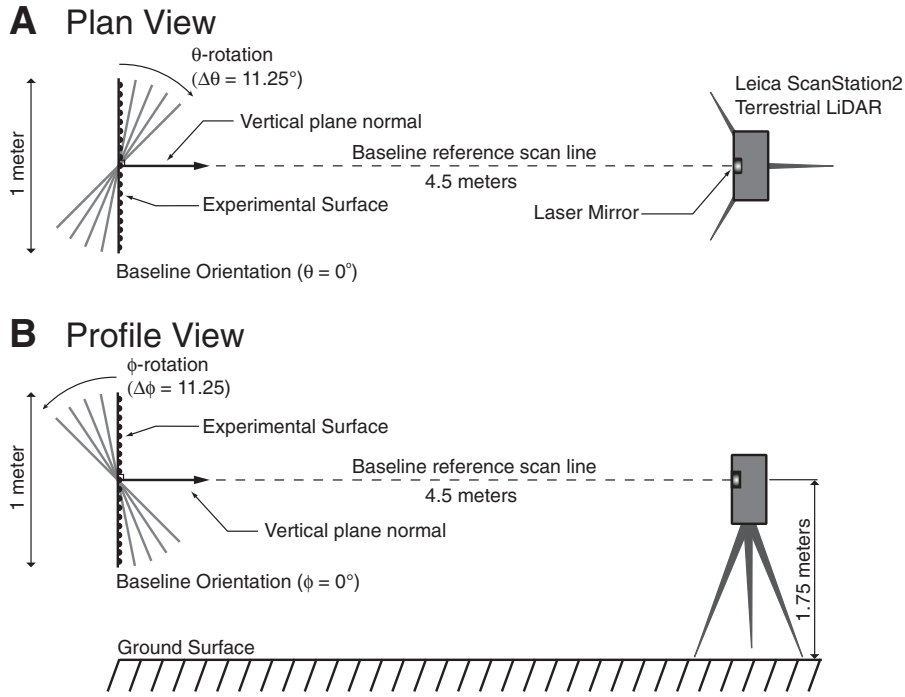

Figure 3. Schematic illustration of the experimental setup and dual-axis surface rotations in (A) plan view and (B) profile view. Surface rotations about the vertical axis are referenced by angle θ (A), and surface rotations about the surface-parallel axis are referenced by angle ϕ (B).

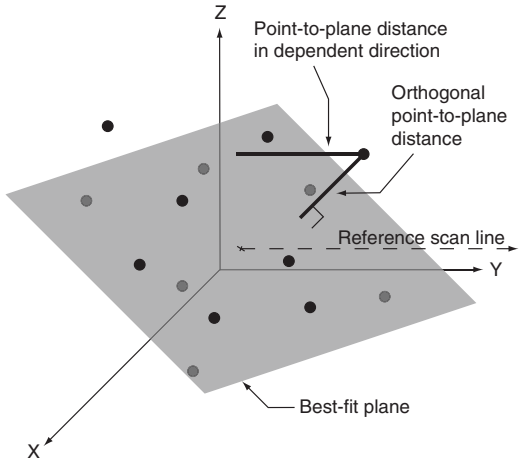

Figure 4. Schematic illustration of the difference between orthogonal point-to-plane distances and those measured with respect to the dependent coordinate axis.

TABLE 1. SURFACE ROUGHNESS RESULTS

ϕ	σ_{ols}	σ_{hyb}	σ_{odr}	N
		θ = 0.0°		
0.0°	0.00394161	0.00394367	0.00394365	245613
11.25°	0.00398452	0.00398661	0.00391173	241176
22.5°	0.00416767	0.00417000	0.00385730	227464
33.75°	0.00452453	0.00452740	0.00379007	206600
45.0°	0.00521033	0.00521427	0.00370090	175124
		θ = 11.25°		
0.0°	0.00397112	0.00397333	0.00389274	239661
11.25°	0.00400794	0.00401010	0.00385206	235784
22.5°	0.00421576	0.00421821	0.00381358	222359
33.75°	0.00461311	0.00461626	0.00376637	199981
45.0°	0.00540323	0.00540777	0.00375125	170004
		θ = 22.5°		
0.0°	0.00413984	0.00414247	0.00380949	225606
11.25°	0.00422216	0.00422485	0.00381041	221026
22.5°	0.00449653	0.00449959	0.00380379	207347
33.75°	0.00487570	0.00487959	0.00374020	188002
45.0°	0.00563781	0.00564332	0.00369239	160422
		θ = 33.75°		
0.0°	0.00452617	0.00452961	0.00374516	202366
11.25°	0.00461460	0.00461816	0.00374334	199235
22.5°	0.00488860	0.00489264	0.00374680	188647
33.75°	0.00534249	0.00534769	0.00369730	170312
45.0°	0.00628228	0.00629044	0.00369400	144099
		θ = 45.0°		
0.0°	0.00521557	0.00522081	0.00368465	173055
11.25°	0.00538243	0.00538789	0.00373105	170268
22.5°	0.00566031	0.00566686	0.00370104	160810
33.75°	0.00626838	0.00627654	0.00372058	146149
45.0°	0.00721824	0.00723020	0.00362923	123103

Note: ϕ—Rotation angle about surface-parallel horizontal axis; θ—rotation angle about vertical axis; σ_{ols}—ordinary least-squares surface roughness mode; σ_{hyb}—hybrid surface roughness model; σ_{odr}—orthogonal distance regression surface roughness model; N—number of points acquired for scan; units for surface roughness are meters.

contrast, the σ_{ols} and σ_{hyb} models return roughness estimates that deviate strongly with increasing angular rotation (Table 1). This effect will be analyzed in the following section.

DISCUSSION

Discussion of the three surface roughness models begins with a direct comparison of σ(0°,0°) for each roughness model, and a comparison of these estimates to the numerically derived theoretical surface roughness (σ_{thr}). The (0°,0°) surface orientation provides the maximum viewable surface area to the laser scanner, which represents the closest experimental approach to the synthetic point cloud generated for the σ_{thr} solution. In addition, the (0°,0°) surface normal is aligned with the dependent coordinate axis, so that the OLS regression is forced to minimize orthogonal distances, thus returning the same best-fit plane as the ODR model. For the same reason, point-to-plane distances measured with respect to the dependent axis are also orthogonal to the regression plane. This implies, mathematically, that each roughness model should return equal σ(0°,0°).

In fact, this is the case here, where the differences between $\sigma_{odr}(0°,0°)$, $\sigma_{ols}(0°,0°)$, and $\sigma_{hyb}(0°,0°)$ are negligible (0.05%); however, a comparison of these surface roughness estimates to the numerically derived theoretical surface roughness (σ_{thr}) reveals an error of 9% common to all three models of surface roughness. This error is an indistinguishable combination of (1) decreasing point density caused by the increasing angle of incidence between the laser scan line and experimental surface during scanner pivot, (2) LiDAR instrument error (single datum position and distance accuracy for the LeicaScanstaion2 are specified as 6 mm and 4 mm, respectively), and (3) imperfections in the constructed experimental surface. This error is shared by all three roughness models, propagated equally into each roughness estimate, and may be considered a constant, but equally distributed error ($_{exp}$) in this analysis.

The $\sigma(\theta,\phi)$ for each roughness model is evaluated against σ_{thr} by removing $_{exp}$ from each estimate and normalizing the values over σ_{thr}:

$$\sigma^*(\theta,\phi) = \frac{\left[\sigma(\theta,\phi) - \ _{exp}\right] - \sigma_{thr}}{\sigma_{thr}}, \quad (3)$$

where $\sigma^*(\theta,\phi)$ is normalized surface roughness. This normalization translates each $\sigma(0°,0°)$ onto the σ_{thr} and scales each $\sigma(\theta,\phi)$ as a fraction representing relative error above or below σ_{thr}. Plots of $\sigma^*(\theta,\phi)$ are presented in Figure 5. The apparent pattern in Figure 5 indicates that σ_{ols} and σ_{hyb} models dramatically overestimate the true experimental surface roughness for increasing (θ,ϕ) rotations, e.g., 17 of the 25 $\sigma^*_{ols}(\theta,\phi)$ and $\sigma^*_{hyb}(\theta,\phi)$ exceed 10% relative error. Additionally, the close agreement with the σ_{ols}

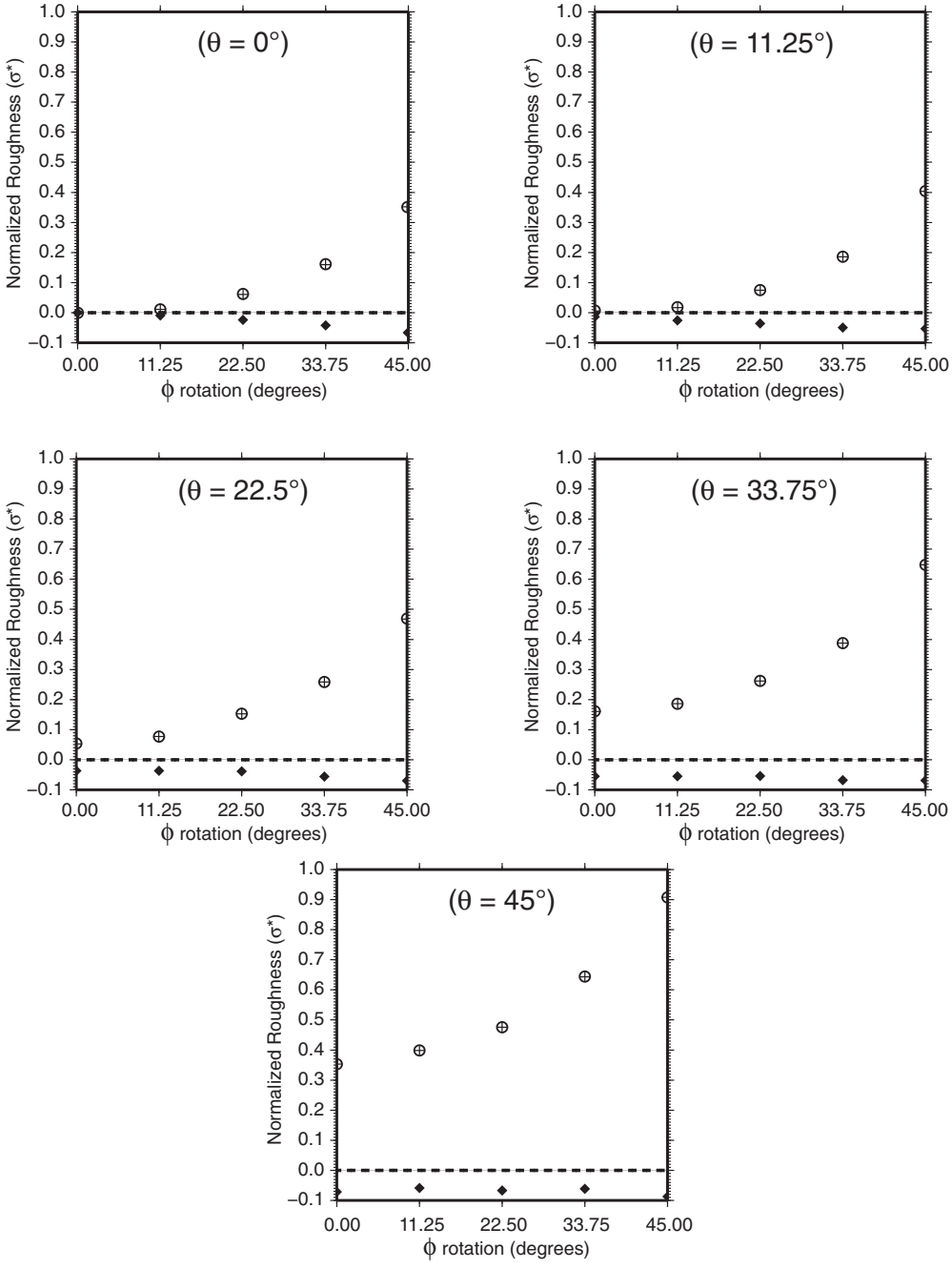

Figure 5. Plots of normalized surface roughness (σ^*) for each θ rotation as a function of ϕ rotation. The σ^* values represent the fraction of relative error above or below the theoretical surface roughness (σ_{thr}), where relative percent error is $\sigma^* \times 100$. The dashed line represents σ_{thr}, which has been normalized to zero. The solid diamonds are the σ^*_{odr} roughness values, open circles are the σ^*_{ols} roughness values, and plus symbols are the σ^*_{hyb} roughness values.

and σ_{hyb} models for all (θ,ϕ) suggests that roughness models are more sensitive to the direction in which point-to-plane distances are measured than to the choice of reference datum. In contrast to the σ_{ols} and σ_{hyb} models, the σ_{odr} model returns roughness estimates consistently below σ_{thr}; however, the percent relative error is less than 10% for all (θ,ϕ) rotations suggesting that σ_{odr} represents a minimum error model for surface roughness. This robustness to surface orientation results from the mathematical properties of the σ_{odr} model and suggests deviations of $\sigma_{odr}(\theta,\phi)$ from σ_{thr} are due to LiDAR sampling error. For this reason, the remainder of this section will focus on the impacts of σ_{odr} to LiDAR sampling errors.

Sampling errors in the LiDAR-based data sets may arise from several, well-documented sources (Liu, 2004; Buckley et al., 2008; Lato et al., 2010); however, the impacts of these errors on surface roughness models have not been addressed. One source of surface roughness error arises from the instrument accuracy, which, for this experiment, is propagated equally into each angular scan and, more generally, may be considered a fixed and irreducible source of error that is inherently instrument specific. Another source of LiDAR sampling error is angular scanning error, which results from increased point acquisition spacing as the angle of incidence increases between the laser scan line and the scanned surface; see, e.g., Lato et al. (2010, Fig. 3). This is the same effect as one of the contributions to error in the $_{exp}$ term; however, angular sampling error is variable and unique to each (θ,ϕ) rotation. In fact, the number of points (N) on the experimental surface decreases for each rotation as a function of cosine, i.e., $N(\theta,\phi) = N(0°,0°)\cos\theta\cos\phi$, and the magnitude of this undersampling occurs at an increasing rate as the angle of incidence increases (Fig. 6). More generally, angular sampling error affects the σ_{odr} model by disproportionately sampling surfaces with lesser angles of incidence to the laser scan line. For example, the effect of angular sampling error can be seen here in Figure 7, where point density decreases from lower right to upper left across the experimental surface at (45°,45°). The result of angular sampling error is that surface roughness models are more heavily influenced by portions of the scanned surface with greater point density.

Another source of sampling error in LiDAR data sets is due to occlusion, or "shadowing," where protrusions on a scanned surface obstruct the line of sight from the instrument—the result of which is undersampling portions of the scanned surface. Occlusion error is most pervasive for this experiment at the surface orientation (45°,45°), where half of each roughness element and the adjacent smooth board are in the shadow (Fig. 7). As the experimental surface is rotated, the maximum out-of-board dimension of the roughness elements is still viewable to the scanner; however, the shadowed (i.e., unsampled) portion of the smooth board becomes larger. This affects the σ_{odr} model by enhancing the weight given to the best-fit plane by the points landing on the roughness elements, thereby creating a reference plane with smaller point-to-plane distances, and consequently, smaller roughness estimates. In other words, for large angular deviation from the baseline surface orientation, the LiDAR is "seeing" a smoother surface than actually exists.

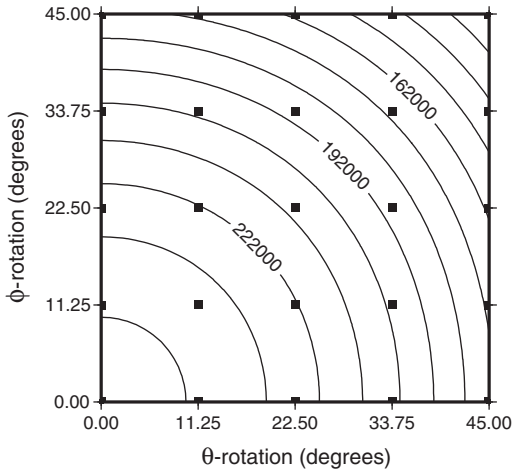

Figure 6. The effects of angular sampling error are shown as contours (solid lines) of the number points (N) landing on the experimental surface as a function of the dual-axis rotation: $N(\theta,\phi) = N(0°,0°)\cos\theta\cos\phi$. The experimental Ns for each (θ,ϕ) rotation are plotted as black squares.

The common approach for fully sampling (removing occlusions from) a scanned surface is to acquire point data from several positions and merge the data sets using stationary targets (Buckley et al., 2008, Fig. 3). This was tested in terms of surface roughness by merging the (45°,45°) data set with a second scan acquired from a survey station located 90° (in plan view) from the original station. This arrangement allowed complete coverage of the experimental surface, providing point data on the previously unsampled portions of the board. The two data sets were merged with a mean registration error of less than 0.001 m and trimmed for stray points as previously described. The σ_{odr} estimate for this merged scan was

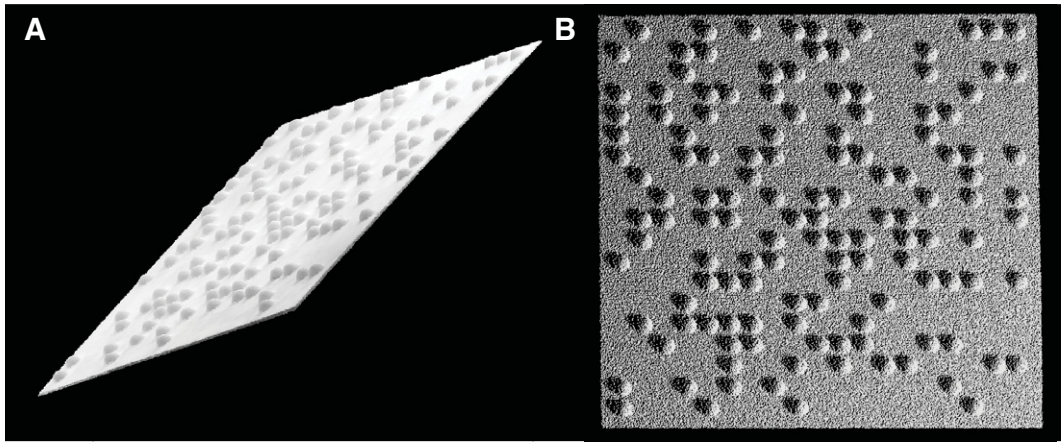

Figure 7. The combined effects of angular and occlusion sampling errors are visualized by (A) comparing a digital image of experimental surface at (45°,45°) viewed from the laser scanner perspective to (B) the associated grayscale intensity map rotated so that the surface normal is out of the page. Occlusion errors are those unsampled portions of the surface up and to the left of each roughness element, whereas angular sampling error is the decreasing point density from lower right to upper left across the surface.

3.67803E-3m and within 1.3% of σ_{odr}(45°,45°). Interestingly, the inability of this merged scan to improve the surface roughness estimate is still a function of occlusion error. This arises because sampling to fill occlusions from the first scan results in new occlusions in the second scan and oversampled portions where the two scans overlap, so the σ_{odr} model gives half as much weight to the "sampled occlusions" than to the unobstructed portions of the surface. Since each of the separate scans contains approximately the same fraction of occluded and non-occluded surface area, the calculated roughness statistics remain nearly identical.

Although some amount of irreducible error exists in all physically based models, the results of this experiment suggest some practical guidance for minimizing errors to which LiDAR-based surface roughness models are prone. The σ_{odr} model is suggested as a robust general tool for LiDAR-based surface roughness estimation. When developing sampling strategies for terrestrial laser scanning, the effects of angular sampling error should be considered. In particular, we recommend positioning LiDAR instrument stations as close to the vertical center and as far back from the scanned surface as possible while maintaining the desired point resolution and intensity of returns. This effectively decreases the range of incident angles between the scan line and scanned surface resulting in more evenly distributed point density. The use of multiple low-angle scans is also recommended; the results in Figure 5 suggest scanning half-angles of 22.5° may keep roughness errors within 5%. Lastly, while it is tempting to sample a given surface from a myriad of directions, the effects of occlusion error on surface roughness estimation may be the most difficult error to reduce. Although sampling an area from multiple directions can fill in surface topography, as shown here it cannot significantly reduce the effects of occlusion error on surface roughness models. Furthermore, ad hoc oversampling can result in collecting a large quantity of redundant data, leading to greater computational expense with little return. Perhaps one practical suggestion for minimizing the effects of occlusion error on surface roughness models is to seek a balance between efficient time management in the field and acquiring multiple segmented (and merged) scans from minimum occlusion orientations, while minimizing overlap. Although this recommendation may have adverse consequences with respect to scan registration errors or areal data coverage, the broader context is that thoughtful, investigation-based consideration should be given to the benefits of oversampling versus the computational expense for data processing.

CONCLUSIONS

In this work we have sought to enhance understanding of surface roughness as a technique for analyzing terrestrial LiDAR data. If the digital terrain model is the primary- or zero-order tool for LiDAR data analysis, then surface roughness may be considered a first-order extension of the LiDAR toolbox. Surface roughness complements the utility of the DTM or similar smoothing function by evaluating the degree of intra-cell point variability about the modeled surface and has proven a useful metric for mapping features lost with DTM smoothing functions. For example, surface roughness has been invoked across a wide range of geoscience disciplines for mapping alluvial fan deposits (Frankel and Dolan, 2007), channel bed morphology (Cavalli et. al., 2008), landslide scarps (McKean and Roering, 2004), and fractures in outcrop (Pollyea and Fairley, 2011). However, despite this widespread appeal, the techniques for its application are far from standardized. The work presented here demonstrates that surface roughness models are sensitive to the orientation of the surface being modeled. For this reason, the surface roughness model based on orthogonal distance regression and orthogonal point-to-plane distance measurements (σ_{odr}) is recommended as a generally robust method for estimating surface roughness. This recommendation does not come without caveat because, as demonstrated here, the σ_{odr} is adversely affected by LiDAR sampling error. Several practical recommendations are provided for minimizing sampling error; these include: (1) positioning the instrument as near the vertical center and as far back from the scanned surface as is practicable, (2) using scanning half-angles less than 22.5°, and (3) minimizing surface occlusion by using multiple segmented (and merged) scans with as little overlap as possible. Surface roughness models provide another step toward unlocking the full potential of LiDAR-derived data sets, and we hope this effort encourages other investigators to seek additional approaches toward this end.

ACKNOWLEDGMENTS

The authors thank Jennifer Hinds for her assistance operating the LiDAR scanner and Gerry Queener for his assistance with the experimental surface specs. This work was supported by a Grant-in-Aid of Research from the National Academy of Sciences, administered by Sigma Xi, The Scientific Research Society (grant G20101015154774) and the Center for Advanced Energy Studies. This manuscript has been greatly improved by the thought-provoking and challenging comments provided by two anonymous reviewers and Associate Editor F. Mazzarini.

REFERENCES CITED

Aberle, J., and Nikora, V., 2006, Statistical properties of armored gravel bed surfaces: Water Resources Research, v. 42, doi:10.1029/2005WR004674.

Bellian, J., Kerans, C., and Jennette, D., 2005, Digital outcrop models: Applications of terrestrial scanning lidar technology in stratigraphic modeling: Journal of Sedimentary Research, v. 75, no. 2, p. 166–176, doi:10.2110/jsr.2005.013.

Buckley, S.J., Howell, J., Enge, H., and Kurz, T., 2008, Terrestrial laser scanning in geology: Data acquisition, processing and accuracy considerations: Journal of the Geological Society of London, v. 165, p. 625–638, doi:10.1144/0016-76492007-100.

Cavalli, M., Tarolli, P., Marchi, L., and Dalla Fontana, G., 2008, The effectiveness of airborne LiDAR data in the recognition of channel-bed morphology: Catena, v. 73, p. 249–260, doi:10.1016/j.catena.2007.11.001.

Fardin, N., Feng, Q., and Stephansson, O., 2004, Application of a new in situ 3D laser scanner to study the scale effect on the rock joint surface roughness: International Journal of Rock Mechanics and Mining Sciences, v. 41, p. 329–335, doi:10.1016/S1365-1609(03)00111-4.

Frankel, K.L., and Dolan, J.F., 2007, Characterizing arid region alluvial fan surface roughness with airborne laser swath mapping digital topographic data: Journal of Geophysical Research, v. 112, doi:10.1029/2006JF000644.

Glenn, N.F., Streuker, D.R., Chadwick, J.D., Thackray, G.D., and Dorsch, S.J., 2006, Analysis of LiDAR-derived topographic information for characterizing and differentiating landslide morphology and activity: Geomorphology, v. 73, p. 131–148, doi:10.1016/j.geomorph.2005.07.006.

Heritage, G.L., and Milan, D.J., 2009, Terrestrial laser scanning of grain roughness in a gravel-bed river: Geomorphology, v. 113, p. 4–11, doi:10.1016/j.geomorph.2009.03.021.

Lato, M.J., Diederichs, M.S., and Hutchinson, D.J., 2010, Bias correction for view-limited Lidar scanning of rock outcrops for structural characterization: Rock Mechanics and Rock Engineering, v. 43, p. 615–628, doi:10.1007/s00603-010-0086-5.

Liu, X., 2004, Airborne LiDAR for DEM generation: Some critical issues: Progress in Physical Geography, v. 31, p. 31–49.

McKean, J., and Roering, J., 2004, Objective landslide detection and surface morphology mapping using high-resolution airborne laser altimetry: Geomorphology, v. 57, p. 331–351, doi:10.1016/S0169-555X(03)00164-8.

Pollyea, R.M., and Fairley, J.P., 2011, Estimating surface roughness of terrestrial laser scan data using orthogonal distance regression: Geology, v. 39, no. 7, p. 623–626, doi:10.1130/G32078.1.

Press, W.H., Teukolsky, S.A., Vetterling, W.T., and Flannery, B.P., 1992, Numerical Recipes in Fortran 77: The Art of Scientific Computing: 2nd Edition, v. 1, Cambridge, UK, Cambridge University Press, 933 p.

Sagy, A., Brodsky, E.E., and Axen, G.J., 2007, Evolution of fault-surface roughness with slip: Geology, v. 35, no. 3, p. 283–286, doi:10.1130/G23235A.1.

Sankey, J.B., Glenn, N.F., Germino, M.J., Gironella, A.I.N., and Thackray, G.D., 2010, Relationships of aeolian erosion and deposition with LiDAR-derived landscape surface roughness following wildfire: Geomorphology, v. 119, p. 135–145, doi:10.1016/j.geomorph.2010.03.013.

Wehr, A., and Lohr, U., 1999, Airborne laser scanning—An introduction and overview: International Society for Photogrammetry and Remote Sensing Journal of Photogrammetry and Remote Sensing, v. 54, p. 68–82, doi:10.1016/S0924-2716(99)00011-8.

Manuscript Received 23 June 2011
Revised Manuscript Received 3 October 2011
Manuscript Accepted 13 October 2011